

Purely-long-range bound states of $\text{He}(2s^3S)+\text{He}(2p^3P)$

V. Venturi, P. J. Leo, E. Tiesinga, and C. J. Williams

*Atomic Physics Division, National Institute of Standards
and Technology, Gaithersburg, Maryland 20899*

I. B. Whittingham

*School of Mathematical and Physical Sciences,
James Cook University, Townsville 4811, Australia*

(Dated: November 1, 2018)

Abstract

We predict the presence and positions of purely-long-range bound states of $^4\text{He}(2s^3S) + ^4\text{He}(2p^3P)$ near the $2s^3S_1 + 2p^3P_{0,1}$ atomic limits. The results of the full multichannel and approximate models are compared, and we assess the sensitivity of the bound states to atomic parameters characterizing the potentials. Photoassociation to these purely-long-range molecular bound states may improve the knowledge of the scattering length associated with the collisions of two ultracold spin-polarized $^4\text{He}(2s^3S)$ atoms, which is important for studies of Bose-Einstein condensates.

I. INTRODUCTION

Photoassociation spectroscopy to purely-long-range molecular bound states has proven a powerful tool for examining the ground state wavefunction of alkali atoms, and for precisely determining s -wave scattering lengths for these systems [1, 2, 3]. In recent years there has been a growing interest in rare-gas atoms, and in particular helium systems. The production of Bose-Einstein condensates of spin-polarized metastable ^4He atoms by two different groups [4, 5] allows one to study the properties of these condensates and provides an improved environment for further investigation of cold collisions of metastable ^4He [6, 7]. Additional valuable information about the metastable ^4He system may be obtainable from photoassociation spectroscopy. Herschbach *et al.* [8] observed bound states that dissociate to the $^4\text{He}(2s\ ^3S_1) + ^4\text{He}(2p\ ^3P_2)$ atomic limit by detecting ions produced by Penning ionization. Broadening of the photoassociation peaks due to Penning ionization did not hinder the observation of the vibrational series. There have been no published theoretical or experimental studies of the $^4\text{He}(2s\ ^3S_1) + ^4\text{He}(2p\ ^3P_{0,1})$ purely-long-range bound states.

In this paper we provide theoretical predictions for binding energies of levels of purely-long-range molecular potentials that dissociate to the $^4\text{He}(2s\ ^3S_1) + ^4\text{He}(2p\ ^3P_{0,1})$ atomic limits. The purely-long-range bound states have inner turning points at internuclear separations larger than $150 a_0$ ($1a_0 = 5.29177 \times 10^{-11}\text{m}$) and primarily depend on the dipole-dipole C_3 coefficient and the fine structure splittings of the 3P atom. These quantities are all determined from atomic properties. The purely-long-range bound states are independent of the short-range form of the interaction potentials. Consequently, there may not be a detectable ion signal from Penning ionization processes, which occur at small internuclear separations, $R < 20 a_0$. We cannot make theoretical predictions for levels that have a short-range contribution, because the multipole expansion of the potentials is not appropriate for $R < 30 a_0$ and no short-range $^4\text{He}(2s\ ^3S) + ^4\text{He}(2p\ ^3P)$ potentials exist. For the remainder of the paper, we implicitly mean ^4He when referring to helium.

II. METHOD

We calculate the molecular eigenfunctions of a multichannel Hamiltonian containing the relative kinetic energy operator, twelve non-relativistic Born-Oppenheimer potentials which

include retardation effects, the atomic spin-orbit interaction of the 3P atom, and a term describing nuclear rotation. The model used is similar to that applied to the alkali systems [3]. The Movre-Pichler model [9] adapted to $^3S + ^3P$ systems yields the adiabatic potentials obtained from diagonalizing, at each internuclear separation, the multichannel potentials that include the dipole-dipole and spin-orbit interactions. In our calculations we have not included Penning ionization or spontaneous emission, which can both be represented as an optical or imaginary potential. The radial extent of the optical potential for Penning ionization is localized well inside the inner turning point of the purely-long-range bound states and therefore has a minor role to play for these states. Spontaneous emission is present at all internuclear separations. However, near the $^3S + ^3P$ dissociation limits the vibrational level spacing is large compared to the atomic spontaneous emission width of 1.63 MHz, and spontaneous emission can therefore be treated perturbatively.

The multichannel Hamiltonian has been set up as described in Ref. [10, 11]. The collision between two helium atoms conserves the total molecular angular momentum J and parity p . The total angular momentum is given by $\mathbf{J} = \mathbf{l} + \mathbf{j}$, where \mathbf{l} is the rotational angular momentum and $\mathbf{j} = \mathbf{L} + \mathbf{S}$. Here \mathbf{L} and \mathbf{S} are the electronic orbital and spin angular momenta and Λ and Σ are their respective projections onto the internuclear axis. The projection of \mathbf{j} onto this axis is $\Omega = \Lambda + \Sigma$. In addition, $\mathbf{j} = \mathbf{j}_a + \mathbf{j}_b$, where \mathbf{j}_a and \mathbf{j}_b are the total angular momenta of the 3S and 3P atoms, respectively. Since ^4He has zero nuclear spin, $p = +$ and $p = -$ parity states correspond to gerade (g) and ungerade (u) states, respectively. The $\sigma = g/u$ labels refer to the inversion symmetry of the electron wavefunctions about the center of charge. Negative-parity bound states have contributions from even partial waves l only. Consequently, photoassociation of two ultracold metastable helium atoms, where s -wave collisions dominate, can only excite ungerade $^3S + ^3P$ bound states.

The twelve Born-Oppenheimer potentials are uniquely labelled by $^{2S+1}\Sigma_\sigma^+$ for $\Lambda = 0$ or $^{2S+1}\Pi_\sigma$ for $|\Lambda| = 1$, where the $+$ superscript denotes the symmetry of the spatial electronic wavefunction with respect to reflection through a plane containing the internuclear axis. For $R > 30 a_0$, the dispersion potentials are given by $f_{3\Lambda}(R/\lambda)C_{3\Lambda}/R^3 + C_{6\Lambda}/R^6$, where $f_{3\Lambda}$ is an R - and Λ -dependent retardation correction [12]. The quantity $\lambda = 3258.17 a_0$, where $\lambda = \lambda/(2\pi)$ and λ is the $2s^3S - 2p^3P$ transition wavelength. The $C_{3\Sigma}$ coefficient is $\pm 2C_3$ and $C_{3\Pi}$ is $\pm C_3$, where C_3 is $6.41022 E_h a_0^3$ [13], E_h is a Hartree, and C_3 is proportional to the square of the $2s^3S - 2p^3P$ transition dipole matrix element. Following the Physical

Reference Database [14], we assume a 1% uncertainty or “extent of the possible error” for this coefficient. The $C_{3\Lambda}/R^3$ contributions to the potentials are attractive for the $^1\Sigma_u^+$, $^3\Sigma_g^+$, $^5\Sigma_u^+$, $^1\Pi_g$, $^3\Pi_u$, and $^5\Pi_g$ states, and repulsive for the $^1\Sigma_g^+$, $^3\Sigma_u^+$, $^5\Sigma_g^+$, $^1\Pi_u$, $^3\Pi_g$, and $^5\Pi_u$ states. The van der Waals coefficients are $C_{6\Sigma} = 2620.76 E_h a_0^6$ and $C_{6\Pi} = 1846.60 E_h a_0^6$ [15]. These can be calculated from atomic dipole moments and transition frequencies [16]. It turns out that the C_3/R^3 term is the dominant contribution to the dispersion potential relevant for the purely-long-range states.

The j_b quantum number for the $2p^3P$ atom, which describes the spin-orbit interaction, has the values 0, 1, or 2. The $2p^3P_0$ and $2p^3P_1$ levels lie 31.9081 GHz and 2.2912 GHz above the $2p^3P_2$ level, respectively [17, 18]. Note that these energy splittings do not satisfy the Landé intervals. The rotational Hamiltonian is given by $\hbar^2 \mathbf{I}^2 / 2\mu R^2$, where $\mu = m/2$ is the reduced mass of the system. The atomic mass is $m = 4.0026032$ u, where $1 \text{ u} = 1.66053873 \times 10^{-27}$ kg.

We investigate the sensitivity of the bound states to the short-range Born-Oppenheimer potentials. No data on the short-range shape currently exists, so we use two different forms for the short-range potentials for $R < 30 a_0$. The first of these short-range forms assumes a hard wall for all twelve potentials at $R = 30 a_0$. For smaller internuclear separations the potentials are no longer described by the dispersion potential. For the second short-range form, the attractive Born-Oppenheimer potentials are given a more realistic Lennard-Jones-like form, with inner turning points between $4 a_0$ and $5 a_0$.

The molecule is best described by the Hund’s case (a) coupling scheme at small R , where the splitting between the Born-Oppenheimer potentials is large compared to the spin-orbit interaction. The molecular states are well described by the quantum numbers J and $^{2S+1}\Lambda_\sigma^\pm$. As the internuclear separation increases and the energy separation between the Born-Oppenheimer curves becomes comparable to the atomic spin-orbit interaction, the Hund’s case (a) coupling scheme becomes less appropriate, and the R -dependent Hund’s case (c) coupling scheme is a more suitable choice for describing the long-range states and potentials. The Hund’s case (c) molecular states are described by the quantum numbers J , Ω_σ^\pm . For $\Omega = 0$ the \pm superscript label denotes the symmetry of the electronic wavefunction with respect to reflection through a plane containing the internuclear axis. We note that for the $\Omega = 0$ states, only 0_u^- and 0_g^+ exist for even J , while the 0_u^+ and 0_g^- states exist for odd J . The Hund’s case (c) states are a linear combination of the Hund’s case (a) states.

Table I gives the Hund’s case (a) states that contribute to a given Hund’s case (c) state.

The purely-long-range states discussed in this paper are in the radial regime described by the Hund’s case (c) coupling scheme. We will discuss various approximations to the full multichannel Hamiltonian used in calculating these states. The adiabatic Movre-Pichler model described previously labels each purely-long-range state by Ω_{σ}^{\pm} . An improvement on this model is the multichannel Hamiltonian that includes the Born-Oppenheimer potentials and the spin-orbit interaction. In addition, we discuss two ways of including the nuclear rotation. These approximate Hamiltonians are useful for assigning vibrational quantum numbers to the bound states calculated using the full multichannel model, and the adiabatic Movre-Pichler model is useful for confirming the assignment of Hund’s case (c) labels to the bound states.

The adiabatic Movre-Pichler potentials are shown in Figs. 1 and 2. They are obtained using an extension of the model defined in Ref. [9]. This extended Movre-Pichler model is adapted to the ${}^3S + {}^3P$ system and, in addition to the usual dipole-dipole and the spin-orbit interactions, includes the C_6/R^6 dispersion term and retardation. As mentioned previously, the fine structure splittings for the He($2p\ {}^3P$) atom do not satisfy the Landé intervals, which results in a coupling between molecular singlet and quintet states. For large R , the potentials in Figs. 1 and 2 dissociate to the three 3P fine structure limits. For smaller R the potentials correlate to attractive and repulsive Born-Oppenheimer potentials, as indicated in the figures. We find a number of purely-long-range potential wells in the adiabaticized potentials dissociating to the $2s\ {}^3S_1 + 2p\ {}^3P_0$ and $2s\ {}^3S_1 + 2p\ {}^3P_1$ atomic limits that can support bound states. In Figs. 1 and 2 the 1_g and 0_u^+ states dissociating to the $2s\ {}^3S_1 + 2p\ {}^3P_0$ limit provide an example of such wells, while the wells in the states dissociating to the $2s\ {}^3S_1 + 2p\ {}^3P_1$ limit are too shallow to be observed on the scale of the present figure. There are no purely-long-range states dissociating to the $2s\ {}^3S_1 + 2p\ {}^3P_2$ limit.

The eigenstates of the Hamiltonian are determined by multichannel bound state calculations in a manner similar to that described in Ref. [3]. Long-range bound states are not “true” bound states of the system when their energy lies above the $2s\ {}^3S_1 + 2p\ {}^3P_2$ dissociation limit. They are bound states embedded in a continuum and consequently can predissociate. In our method a hard wall is placed at a large internuclear separation, $R > 5000 a_0$. Consequently, the calculated states are either bound states or “box states”, which characterize the continuum. These two types of states are distinguished by visual inspection of a multi-

channel eigenvector $|\Psi(R)\rangle = \sum_i \psi_i(R)|i\rangle$ or the square root of the density $(\sum_i |\psi_i(R)|^2)^{1/2}$, where the sum is over a finite number of molecular spin states $|i\rangle$. The function ψ_i is the radial component for spin state $|i\rangle$, which is characterized by the total spin, parity, and other angular momenta. The two types of states can also be distinguished by their sensitivity to the location of the hard wall boundary condition. The predissociation of the bound states will be further discussed in the next section.

III. RESULTS

Four sets of purely-long-range ro-vibrational states are found in the multichannel analysis and the binding energies for these levels are given in Table II. We report here only levels with binding energies greater than 1 MHz even though states bound by less than twice the atomic line width, 3.25 MHz, may not be clearly observable. The levels are characterized using Hund's case (c) labels. The 1_g and 0_u^+ potentials dissociating to the $2s^3S_1 + 2p^3P_0$ limit and the 0_u^- and 2_u potentials dissociating to the $2s^3S_1 + 2p^3P_1$ limit have purely-long-range states. Each of these potentials has no more than 6 vibrational levels. These levels are labelled by v and exhibit a rotational progression when $J \geq \Omega$. In addition, 0_u^+ (0_u^-) states only exist for J odd (even). The uncertainty in the binding energy due to changing the short-range Born-Oppenheimer potentials is negligible. The last significant digit of the binding energy indicates the predissociation width, an estimate of which is obtained by comparing the energies for varying locations of the hard wall at large R . We find the predissociation width is on the order of, or smaller than, the natural line width. Gerade/ungerade symmetry states can only be formed by photoassociation via odd/even partial wave collisions. At the internuclear separations of relevance to the states described here, retardation corrections that introduce dipole-forbidden coupling between gerade and ungerade states [19] are small.

As shown in Table II for the lowest allowed rotational level of each state, the 1% extent of the error on C_3 produces a change of less than 1 MHz for the 1_g bound states dissociating to the $2s^3S_1 + 2p^3P_0$ limit and the 0_u^- and 2_u bound states dissociating to the $2s^3S_1 + 2p^3P_1$ limit. For the 0_u^+ bound states dissociating to the $2s^3S_1 + 2p^3P_0$ limit, changes of up to 4 MHz are found for the $v = 0$ to $v = 3$ levels. The higher vibrational levels are shifted by less than 1 MHz. These changes are obtained using a fixed location of the hard wall at large R . It is necessary to include retardation as it leads to a small correction in the binding energy.

For the deepest purely-long-range potential, the 0_u^+ dissociating to the $2s^3S_1 + 2p^3P_0$ limit, the retardation correction lowers the bound state energy of the $J = 1, v = 0$ ro-vibrational level by approximately 7 MHz. The complete C_6/R^6 contribution to the bottom of this 0_u^+ well at $R \approx 190 a_0$ is approximately 0.4 MHz. Therefore the shift in the binding energy due to any uncertainty in C_6 is small compared with the natural line width.

We look at three examples to clarify the ro-vibrational and Hund's case (c) assignments of the levels reported in Table II. In Fig. 3 we show the binding energies for $J = 2, v = 0$ to $v = 3$ ro-vibrational levels of the 2_u state dissociating to the $\text{He}(2^3S_1)+\text{He}(2^3P_1)$ limit for four approximations and the exact multichannel calculation. The four approximations are: (A) the adiabatic extended Movre-Pichler approximation, (B) a non-rotating multichannel calculation including the Born-Oppenheimer potentials and the atomic spin-orbit interaction, (C) an adiabatic calculation of the full $J = 2$ Hamiltonian where the Coriolis coupling between different Ω_u^\pm states has been set to zero, and (D) a multichannel calculation of the full $J = 2$ Hamiltonian where the Coriolis coupling between different Ω_u^\pm states has been set to zero. The binding energies labelled by (E) are obtained using a multichannel calculation of the full $J = 2$ Hamiltonian. All four approximations predict the correct binding energies to within 10%. Experiments are sufficiently accurate that the full multichannel model must be used. For the $v = 0$ level, the 4.9 MHz difference between approximations (A) and (B) is due to the positive diagonal non-adiabatic coupling, which depends on the Born-Oppenheimer and spin-orbit interactions [20]. The 21 MHz discrepancy between the two adiabatic approximations (A) and (C) for the $v = 0$ level can qualitatively be understood by the perturbative inclusion of the $\hbar^2 \mathbf{I}^2 / (2\mu R^2)$ rotational Hamiltonian. For this Hund's case (c) 2_u state the \mathbf{I}^2 of the rotational Hamiltonian simplifies to $J(J+1) - 2\Omega^2 + j(j+1) = J(J+1) - 2$, since $j = \Omega = 2$ near the $\text{He}(2^3S_1)+\text{He}(2^3P_1)$ dissociation limit. Clearly, for the lowest rotational level $J = 2$, a non-zero rotational correction occurs. A non-perturbative calculation is needed for a quantitative understanding of the discrepancy between the two adiabatic approximations (A) and (C) as rotational distortions are important. Similar to the difference between approximations (A) and (B), the difference between approximations (C) and (D) is also due to a positive diagonal non-adiabatic coupling, which now depends on the rotational Hamiltonian as well as the Born-Oppenheimer and spin-orbit interactions. In this case, the comparison of approximation (D) with (E) shows that the coupling between Ω states shifts the $J = 2, 2_u$ levels by no more than 0.5 MHz. Similar comparisons can be obtained for all

of the purely-long-range states.

In Fig. 4 we show the square root of the density for exact $J = 2$ multichannel wavefunctions assigned with the 2_u and 0_u^- symmetries. Also shown are the 2_u and 0_u^- adiabatic potentials dissociating to the $2s^3S_1 + 2p^3P_1$ limit, as obtained using the approximation (C) described previously. These bound levels are purely-long-range because the square roots of the densities show no amplitude for $R < 250 a_0$. In addition, the square roots of the densities calculated using the full multichannel and adiabatic models do not deviate appreciably. A clear vibrational progression from the $v = 0$ to the $v = 1$ level of the 2_u state is visible.

The square root of the density calculated using the full Hamiltonian for three $J = 1, 1_g$ bound levels and two $J = 1, 1_g$ adiabatic potentials dissociating to the $2s^3S_1 + 2p^3P_1$ limit are shown in Fig. 5. The two potentials are calculated using approximation (C). The “deep” 1_g potential has a double-well structure with a minimum at $\approx 315 a_0$. The other “shallow” potential has a minimum at $\approx 530 a_0$. These levels have not been tabulated in Table II because they are sensitive to the short-range potentials. We present them here as they are seemingly purely-long-range except for the penetration of the wavefunction through the barrier of the double-well potentials. The peak of the barrier lies slightly above the $2s^3S_1 + 2p^3P_1$ dissociation limit. The “shallow” potential is not a purely-long-range potential because of significant non-adiabatic mixing with the “deep” 1_g potential. This short-range dependence leads to an uncertainty in the level locations and possible broadening by Penning ionization processes. In addition, the square root of the density for the $v = 0$ level has an oscillatory behavior for $R > 700 a_0$. The periodicity of these oscillations corresponds to the periodicity of the square root of the density for box states in close proximity to the $v = 0$ level. For these 1_g states the amplitude of the oscillations is primarily determined by the rotational coupling. These oscillations indicate significant predissociation.

IV. CONCLUSION

We have predicted the binding energies of all four sets of purely-long-range ro-vibrational levels of ${}^4\text{He}(2s^3S) + {}^4\text{He}(2p^3P)$ potentials dissociating to the $2s^3S_1 + 2p^3P_{0,1}$ fine structure limits. A comparison of the results calculated using the full multichannel and approximate models demonstrates that the full multichannel Hamiltonian is required for accurate comparison with experiment. Retardation and the van der Waals C_6 interaction are found to give

rise to small corrections in the binding energies. We show that a measurement of the binding energy to at least 1 MHz leads to a 1% determination of the dipole-dipole C_3 coefficient.

The current measurements of the $^5\Sigma_g^+$ scattering length of colliding metastable ^4He atoms are $300 \pm 150 a_0$ [5] and $380 \pm 190 a_0$ [4]. This implies that a node in the scattering wavefunction can be found between $150 a_0$ and $600 a_0$ [3]. The inner and outer turning points of our purely-long-range bound states approximately fall within this range of internuclear separations. Consequently the intensity patterns as a function of vibrational level in photoassociation spectroscopy may provide an improved measurement of the scattering length.

The experimental and theoretical binding energies for the 0_u^+ state dissociating to the $2s^3S_1 + 2p^3P_1$ limit reported in Ref. [21] came to our attention upon the completion of this paper. Our theoretical predictions are within the experimental uncertainty for the $v = 1 - 4$ levels and for the $v = 0$ level our theoretical prediction of -1418.1 MHz is 2 MHz greater than the upper bound on the experimental binding energy -1430 ± 10 MHz.

-
- [1] P.D. Lett, P.S. Julienne, and W.D. Phillips, *Annu. Rev. Phys. Chem.* **46**, 423 (1995).
 - [2] W.C. Stwalley and H. Wang, *J. Mol. Spect.* **195**, 194 (1999).
 - [3] E. Tiesinga *et al.*, *J. Res. Natl. Inst. Stand. Technol.* **101**, 505 (1996).
 - [4] A. Robert *et al.*, *Science* **292**, 461 (2001).
 - [5] F. Pereira Dos Santos *et al.*, *Phys. Rev. Lett.* **86**, 3459 (2001); F. Pereira Dos Santos *et al.*, *Eur. Phys. J. D* **19**, 103 (2001).
 - [6] O. Sirjean *et al.*, *Phys. Rev. Lett.* **89**, 220406 (2002); S. Seidelin *et al.*, *J. Opt. B* **5**, S112 (2003).
 - [7] M. Leduc *et al.*, *Acta Phys. Polon. B* **33**, 2213 (2002).
 - [8] N. Herschbach *et al.*, *Phys. Rev. Lett.* **84**, 1874 (2000); G. Woestenenk, Ph.D. Thesis, Utrecht University, 2001.
 - [9] M. Movre and G. Pichler, *J. Phys. B* **10**, 2631 (1977).
 - [10] S. J. Singer, K. F. Freed, and Y. B. Band, *J. Chem. Phys.* **79**, 6060 (1983).
 - [11] B. Gao, *Phys. Rev. A* **54**, 2022 (1996).
 - [12] W. J. Meath, *J. Chem. Phys.* **48**, 227 (1968).
 - [13] G. W. F. Drake (private communication).

TABLE I: The combinations of Hund’s case (a) states which contribute to a given case (c) state, for a particular $\sigma = g/u$ symmetry.

case (c) state	case (a) states
3_σ	$^5\Pi_\sigma$
2_σ	$^5\Pi_\sigma, ^3\Pi_\sigma, ^5\Sigma_\sigma^+$
1_σ	$2 \times (^5\Pi_\sigma), ^3\Pi_\sigma, ^1\Pi_\sigma, ^5\Sigma_\sigma^+, ^3\Sigma_\sigma^+$
0_σ^+	$^5\Pi_\sigma, ^3\Pi_\sigma, ^5\Sigma_\sigma^+, ^1\Sigma_\sigma^+$
0_σ^-	$^5\Pi_\sigma, ^3\Pi_\sigma, ^3\Sigma_\sigma^+$

- [14] NIST Physical Reference Database, <http://physics.nist.gov/PhysRefData>.
- [15] M. Marinescu (private communication).
- [16] P. Kharchenko, J. F. Babb, and A. Dalgarno, Phys. Rev. A **55**, 3566 (1997).
- [17] J. Castilleja *et al.*, Phys. Rev. Lett. **84**, 4321 (2000).
- [18] M. C. George, L. D. Lombardi, and E. A. Hessels, Phys. Rev. Lett. **87**, 173002 (2001).
- [19] M. Machholm, P. S. Julienne, and K.-A. Suominen, Phys. Rev. A **64**, 033425 (2001).
- [20] K. M. Jones *et al.*, Euro. Phys. Lett. **35**, 85 (1996).
- [21] J. Léonard *et al.*, Report No. cond-mat/0304446.

TABLE II: Purely-long-range bound state energies in units of MHz, relative to the dissociation limit of the Hund's case (c) state. v and J are the vibrational and rotational quantum numbers. The bound states for $J \leq 3$ are calculated, and the blank columns indicate that the states do not exist for particular J . The last column, ΔE_v , indicates the change in binding energy of the lowest rotational level for a +1% change in the C_3 coefficient. All binding energies are calculated using the full multichannel model.

Symmetry \rightarrow dissociation limit	v	$J = 0$	$J = 1$	$J = 2$	$J = 3$	ΔE_v
$1_g \rightarrow 2s^3S_1 + 2p^3P_0$	0		-207.66	-170.92	-115.73	0.62
	1		-43.80	-28.52	-7.97	0.47
	2		-4.12			0.13
$0_u^+ \rightarrow 2s^3S_1 + 2p^3P_0$	0		-1418.1		-1212.7	2.4
	1		-649		-513	3
	2		-253.12		-174.5	2.5
	3		-79.65		-41.6	1.35
	4		-18.30		-4.6	0.53
	5		-2.59			0.13
$0_u^- \rightarrow 2s^3S_1 + 2p^3P_1$	0	-18.27		-7.77		0.08
$2_u \rightarrow 2s^3S_1 + 2p^3P_1$	0			-191	-167	0.5
	1			-72	-57	0.6
	2			-21.5	-14.4	0.2
	3			-4.7	-2.2	0.1

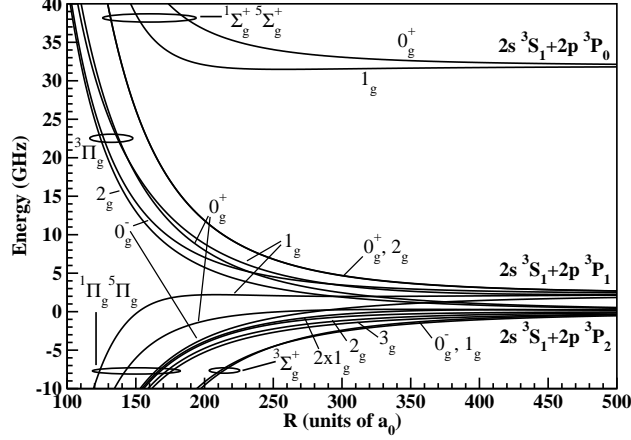


FIG. 1: Adiabatic extended Morse-Pichler potentials of gerade symmetry as a function of internuclear separation. The zero of energy is the $\text{He}(2s^3S_1)+\text{He}(2p^3P_2)$ atomic limit. The potentials are labelled by Ω_g^\pm . At short-range we have indicated with ellipses the $^{2S+1}\Lambda_g^+$ correlations.

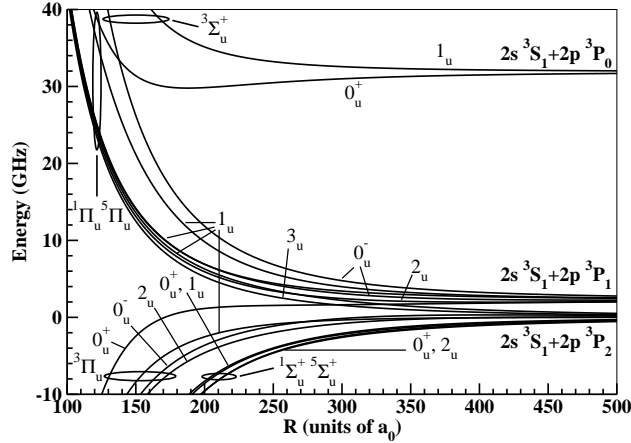


FIG. 2: Adiabatic extended Morse-Pichler potentials of ungerade symmetry as a function of internuclear separation. The zero of energy is the $\text{He}(2s^3S_1)+\text{He}(2p^3P_2)$ atomic limit. The potentials are labelled by Ω_u^\pm . At short-range we have indicated with ellipses the $^{2S+1}\Lambda_u^+$ correlations.

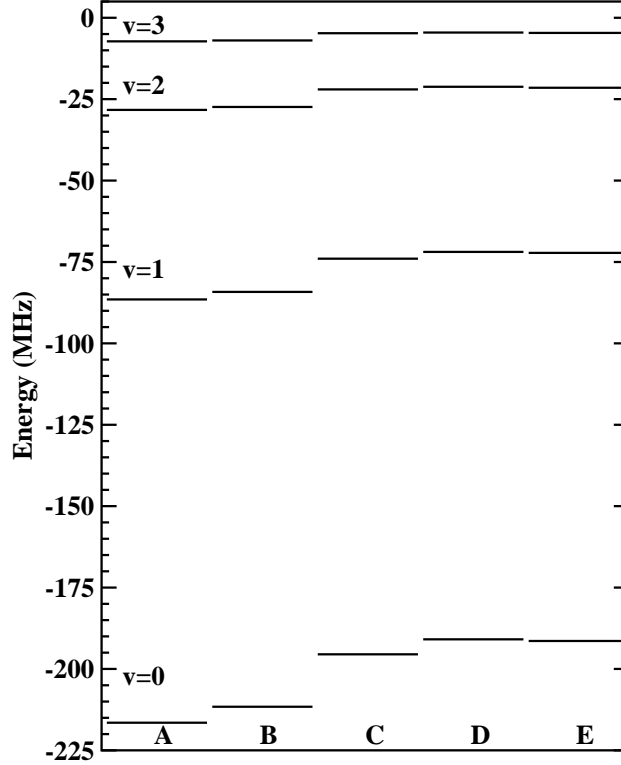


FIG. 3: The binding energy of the $v = 0$ to $v = 3$ vibrational levels of the purely-long-range 2_u potential dissociating to the $\text{He}(2s^3S_1)+\text{He}(2p^3P_1)$ limit. Various approximations to the complete multichannel model are shown. Working from a basic model and increasing in complexity to the complete multichannel calculation: (A) the adiabatic extended Movre-Pichler approximation, (B) a multichannel calculation including the Born-Oppenheimer potentials and the atomic spin-orbit interaction, (C) an adiabatic calculation of the full $J = 2$ Hamiltonian where the Coriolis coupling between different Ω_u^\pm states has been set to zero, (D) a multichannel calculation of the full $J = 2$ Hamiltonian where the Coriolis coupling between different Ω_u^\pm states has been set to zero, and (E) the complete $J = 2$ multichannel calculation.

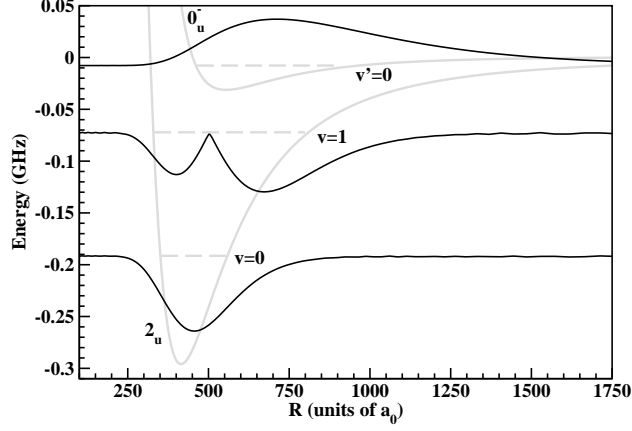


FIG. 4: The square root of the density for the $J = 2$, $v = 0$ and $v = 1$ ro-vibrational levels of the 2_u state and the $J = 2$, $v' = 0$ ro-vibrational level of the 0_u^- state. Note that for the lower two levels the square root of the density curves have been inverted to maintain the distinguishability of the curves. The solid grey curves represent the adiabatic $J = 2$, 2_u and 0_u^- potentials dissociating to the $\text{He}(2s^3S_1)+\text{He}(2p^3P_1)$ limit. The binding energies of the levels are illustrated by dashed horizontal lines.

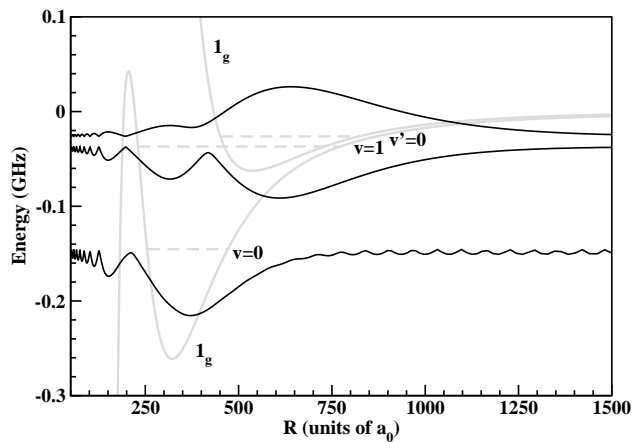


FIG. 5: The square root of the density for the $J = 1$, $v = 0$ and $v = 1$ ro-vibrational levels of the deep 1_g state and the $J = 1$, $v' = 0$ ro-vibrational level of the shallow 1_g state. Note that for the lower two levels the square root of the density curves have been inverted to maintain the distinguishability of the curves. The solid grey curves represent the adiabatic $J = 1$, 1_g potentials dissociating to the $\text{He}(2s\ ^3S_1) + \text{He}(2p\ ^3P_1)$ limit. The density shows significant amplitude for internuclear separations less than $200 a_0$. The binding energies of the levels are illustrated by dashed horizontal lines.